Construction and Building Materials 218 (2019) 543–555

Contents lists available at ScienceDirect

Construction and Building Materials

journal homepage: www.elsevier.com/locate/conbuildmat

On the use of blast-furnace slag in sprayed concrete applications

Renan P. Salvador [a,b,*], Dimas A.S. Rambo [b], Roberto M. Bueno [b], Kaio T. Silva [b], Antonio D. de Figueiredo [a]

[a] Department of Civil Construction Engineering, Polytechnic School of University of São Paulo, Professor Almeida Prado Av, Trav 2, 83, 05424-970 São Paulo, Brazil
[b] Department of Civil Engineering, São Judas Tadeu University, 546 Taquari St., 03166-000 São Paulo, Brazil

HIGHLIGHTS

- Sprayed concrete containing slag reaches strength requirements of classes J_1 and J_2.
- Accelerators activate slag and the matrix achieves a proper hydration behavior.
- Slag does not influence hydration negatively after 3 h when accelerators are added.

ARTICLE INFO

Article history:
Received 12 February 2019
Received in revised form 14 May 2019
Accepted 19 May 2019
Available online 30 May 2019

Keywords:
Sprayed concrete
Blast-furnace slag
Accelerator
Hydration
Mechanical properties

ABSTRACT

Cement replacement by additions is crucial to produce sprayed concrete with proper mechanical properties and durability. The use of blast-furnace slag to produce sprayed concrete for tunnel linings may be restricted due to its low reactivity. In this context, the objective of this study is to evaluate the chemical and mechanical properties of sprayed concrete produced with cement and blast-furnace slag as a partial cement replacement. Hydration kinetics were characterized by isothermal calorimetry, X-ray diffraction and evolution of temperature, while mechanical properties were evaluated by needle penetration resistance and compressive strength of extracted cores. Results showed that slag was activated by the accelerators employed and the minimum strength specified for a J_2 class from 10 to 60 min and at 24 h was achieved. Therefore, blast-furnace slag may be used in sprayed concrete applications when the average strength evolution class is specified.

1. Introduction

Sprayed concrete is a construction technique used worldwide in underground constructions due to technical and economic advantages over conventional concrete [1,2]. Approximately 22.8 million cubic meters of sprayed concrete are expected to be used in the year 2020 and around 37% of that amount will be consumed in tunneling and mining projects in Europe [3]. The high demand of sprayed concrete is promising and, therefore, research and development on this subject are a current need.

In tunnel lining applications, a fast rate of strength development at early ages is often required to ensure the stability of the excavation [1,4,5]. The Austrian Guideline [6] specifies strength evolution classes for sprayed concrete according to the demand of ground support. Compressive strength values for classes J_1, J_2 and J_3 are presented in Fig. 1.

In order to achieve such strength, cement contents around 400 kg/m^3 and accelerator dosages around 5–8% by cement weight are usually employed [7–9]. CEM I 52.5R is the main cement employed due to its fast hydration rates at early ages [1,7]. The compatibility between cement and accelerator is the main parameter that governs the mechanical strength of the matrix at early ages [10].

The use of CEM I provides high early strength, but the mechanical properties and durability at late ages may be compromised [11]. As this cement presents a high reactivity, the matrix sets right after spraying [10,12]. Therefore, sprayed matrices containing accelerators do not consolidate properly and present higher values of water accessible porosities than conventional matrices without accelerators [1,10]. In addition, the heat generated during hydration may form cracks, leading to an overall reduction of the durability of the matrix.

In order to overcome these limitations, limestone filler and silica fume are commonly employed to substitute around 10–15% of the cement content to produce sprayed concrete [1,10]. Blast-furnace slag is not frequently used when compared to limestone

* Corresponding author at: Department of Civil Engineering, São Judas Tadeu University, 546 Taquari St., 03166-000 São Paulo, Brazil.
E-mail address: prof.renansalvador@usjt.br (R.P. Salvador).

https://doi.org/10.1016/j.conbuildmat.2019.05.132
0950-0618/

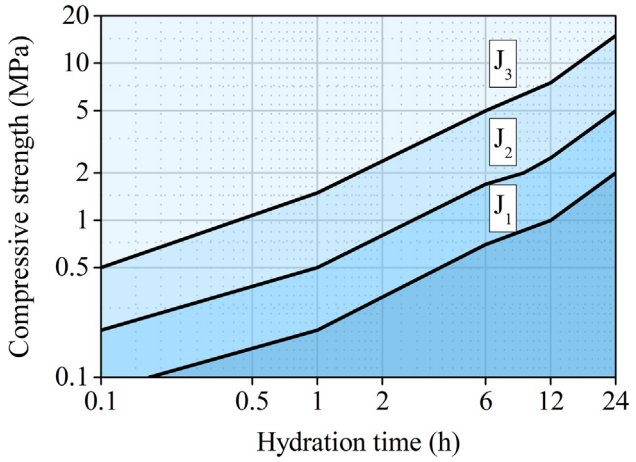

Fig. 1. Compressive strength evolution for sprayed concrete at early ages [6].

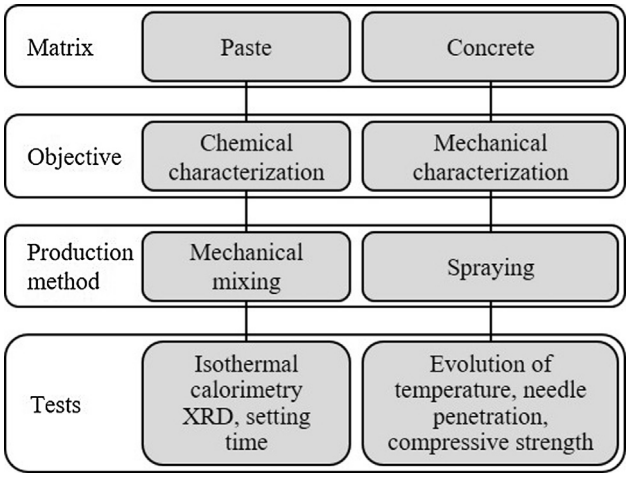

Fig. 2. Scheme of the experimental program conducted in this study.

filler and silica fume due to its low reactivity and mechanical strength evolution at early ages [13], which is a major concern regarding safety in tunnel excavation fronts. In addition, slag compatibility with accelerators based on aluminum sulfate and sodium aluminate, currently employed in structural applications [1,10], needs to be characterized in order to properly specify blast-furnace slag for sprayed concrete.

The use of mineral additives may enhance the pumpability of the matrix because of their fineness and lower density. When slag is employed as cement replacement, the heat generated during hydration reduces, decreasing the risk of cracking [14]. In addition, slag may be activated by accelerators used in sprayed concrete, enhancing hydration kinetics and increasing strength at early ages [15]. From the sustainability point-of-view, CO_2 emissions may be reduced by 33% when cement is replaced by slag in sprayed concrete applications, since it is and industrial byproduct [15–17].

In this context, the objective of this study is to evaluate the use of blast-furnace slag in sprayed concrete for structural applications, focusing on slag reactivity with accelerators and its effect on mechanical strength evolution. An experimental program was conducted to characterize chemical and mechanical properties of accelerated cementitious matrices containing slag. Kinetics and mechanisms of hydration were characterized by isothermal calorimetry, X-ray diffraction and evolution of temperature. The development of mechanical strength was evaluated by needle penetration resistance and compressive strength of extracted cores. Results obtained indicate that slag is activated by the accelerators used and the resulting matrix fulfils the requirements of the strength class J_2. Therefore, blast-furnace slag may be considered as a supplementary cementitious material in sprayed concrete applications when the average strength evolution class is specified.

This paper belongs to a publication series from the research team and some information of previous published works are used for comparison purposes.

2. Experimental methodology

This research was conducted at the Laboratory of Civil Construction Engineering from University São Judas and at the Laboratory of Materials, Components and Construction Processes from the Polytechnic School of University of São Paulo, both in Brazil. The scheme adopted for the experimental program conducted in this study is presented in Fig. 2. The chemical characterization was performed in cement pastes to avoid the dilution of pastes by aggregates. On the other hand, mechanical characterization was conducted in specimens produced with sprayed concrete.

2.1. Materials

The cementitious materials employed were a type I Portland cement (CEM I 52.5R) and a ground granulated blast-furnace slag. Table 1 shows their chemical composition determined by XRF spectrometry and Table 2 presents the mineralogical composition of CEM I determined by XRD-Rietveld refinement using the external standard method [18]. It was not possible to determine the mineralogical composition of the blast-furnace slag because the XRD pattern obtained revealed only a large amorphous halo from 20 to 37 °2θ, as observed in Fig. 3. The chemical and physical properties of both materials are summarized in Table 3.

For the production of cement pastes, distilled water and a superplasticizer based on a polycarboxylate solution (34% of solid

Table 1
Chemical composition of CEM I and blast-furnace slag determined by XRF spectrometry.

Compound	CEM I 52.5R (%)	Blast-furnace slag (%)
LOI	3.08	0.76
CaO	64.30	41.72
SiO_2	19.76	37.10
Al_2O_3	4.68	11.52
Fe_2O_3	3.01	0.89
SO_3	2.49	0.94
MgO	1.33	5.71
K_2O	0.86	0.50
Na_2O	0.32	0.22
Minor components	0.17	0.64
Total sum	100.0	100.0

Table 2
Mineralogical composition of CEM I determined by XRD / Rietveld refinement.

Compound	CEM I 52.5R (%)
C_3S	66.4
C_2S	8.9
C_3A_c	3.4
C_3A_o	0.7
C_4AF	10.8
CaO	0.4
$CaCO_3$	5.4
$CaSO_4{\cdot}2H_2O$	1.1
$CaSO_4{\cdot}0.5H_2O$	2.9
Total sum	100.0

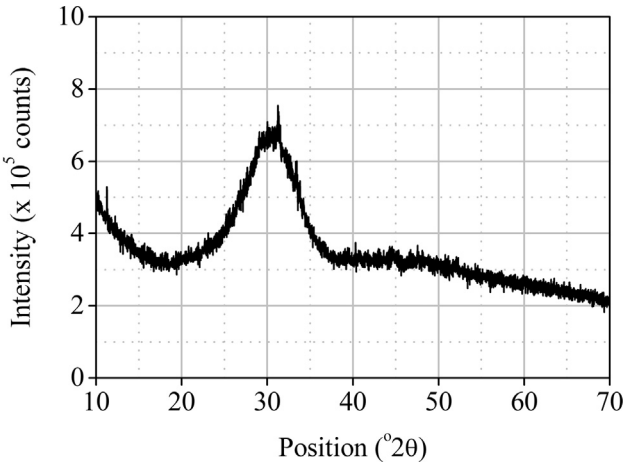

Fig. 3. XRD pattern obtained with the blast-furnace slag.

Table 3
Chemical and physical properties of CEM I and blast-furnace slag.

Property	CEM I 52.5R (%)	Blast-furnace slag (%)
Total heat of hydration[a] (J/g)	451.2	–
C_3A/SO_3 molar ratio	0.58	–
Insoluble residue (%)	0.80	1.41
Specific surface BET (m^2/g)	1.39	0.64
d_{10} (μm)	2.34	1.67
d_{50} (μm)	15.71	13.38
d_{90} (μm)	41.49	37.84

[a] The total heat of hydration was estimated from the mineralogical composition of the cement, determined by XRD, as the relative sum of the heats of hydration of the individual phases (C_3S: 510 J/g; C_2S: 260 J/g; C_3A: 1100 J/g; C_4AF: 410 J/g [19]).

content) were used. One alkali-free accelerator (AF) composed by an aluminum hydroxysulfate solution and an alkaline accelerator (AK) based on sodium aluminate were selected to cover the types commonly found in practice. Table 4 presents their properties.

For the production of concrete, a plasticizer based on a lignosulphonate solution (21% solid content), a superplasticizer based on a polycarboxylate solution (34% solid content) and a retarder composed by a sucrose derivative (28% solid content) were employed. The combination of these three admixtures was necessary to control the workability and the setting of the concrete matrix. Retarders interact with calcium ions in solution, slowing down the building up of the supersaturation needed for the nucleation of hydrates. Therefore, retarders delay portlandite precipitation and, consequently, the formation of C—S—H [20]. Their use in sprayed concrete may affect the early strength development of the matrix (until 2–3 days), although strength at late ages (after 28 days) may not be negatively influenced [20].

Accelerators types and dosages used to produce sprayed concrete were the same as the ones employed in cement pastes

Table 4
Properties of accelerators.

Property	AF	AK
Solid content (%)	40.0	43.0
Specific weight (g/cm^3)	1.32	1.45
pH at 20 °C	2.5	13.0
Al_2O_3 content (%)[a]	11.2	24.0
SO_4^{2-} content (%)	27.6	–
Na_2O content (%)	–	19.0
Al_2O_3/SO_4^{2-} molar ratio	0.38	–
Stabilizing agent	organic acid	–

[a] Al_2O_3 corresponds to Al^{3+} and $[Al(OH)_4]^-$ in AF and AK, respectively.

Table 5
Properties of aggregates employed to produce concrete.

Aggregate	Particle size distribution (mm)	Specific weight (g/cm^3)	Unit weight (g/cm^3)
Fine sand	0–1.20	2.614	1.493
Coarse sand	0–4.75	2.676	1.575
Gravel	4.75–12.5	2.672	1.379

(Table 4). Three types of siliceous aggregates were used to produce concrete. Their properties are described in Table 5. The combination of these aggregates was necessary to provide an adequate flowability and to reduce rebound during the spraying operation.

2.2. Composition and preparation of cement pastes and concrete

The composition and preparation of cement pastes and concretes are presented in Sections 2.2.1 and 2.2.2. Reference matrices do not contain accelerators and are named as *'REF'*. Accelerated matrices are identified by *'accelerator name and dosage'*.

2.2.1. Pastes

Pastes were produced with a fixed water/cementitious material (w/cm) ratio equal to 0.45 and 0.7% of superplasticizer by cementitious material weight (% bcmw). Accelerator AF was used at 6.0 and 8.0% bcmw, while accelerator AK was added at 2.0 and 4.0% bcmw. These dosages fall within the limits usually employed in tunnels executed with sprayed concrete. They were determined according to [1] to guarantee equivalent mechanical performance in pastes.

The combinations of cementitious materials employed in pastes were prepared in laboratory. For isothermal calorimetry, four types were prepared, which were composed by CEM I 52.5R with 0, 15, 30 and 45% of blast-furnace slag in substitution of cement. This range was adopted in order to reach a more complete characterization of the hydration kinetics when different amounts of blast-furnace slag are employed. This evaluation was possible because the amount of cement necessary for each test was 75.00 g.

Since 2 tons of cement were necessary for the application of sprayed concrete, field tests were limited to use the compound cement that was commercially available in Brazil. The only combination employed was composed by 70% CEM I 52.5R and 30% blast-furnace slag. This compound cement may be classified as a CEM II/B-S 42.5 R, according to [21]. Therefore, in order to provide the phase evolution characterization of this system, XRD was also performed with this cement type.

For the preparation of cement pastes, cement and blast-furnace slag were pre-mixed, added to water and homogenized for 1 min using an IKA RW 20 agitator coupled with a R1342 4-bladed stirrer at 1500 rpm in a 500 mL plastic beaker. Then, superplasticizer was added and the mixture was homogenized for 1 min at 1500 rpm. After that, the paste was stored in a climatic chamber, where it was kept at 23 °C for 1 h. Finally, the paste was homogenized again for 30 s at 1500 rpm and accelerators were added using a syringe. The resulting mix was homogenized for 30 s at 1500 rpm and destined to the respective tests. The addition of accelerator 1 h after the initial mixing intends to reproduce the condition found in sprayed concrete in practice (notice that concretes must be transported to the worksite after mixing, where they are sprayed with accelerators). This procedure also contributes to a clearer assessment of the heat flow attributed to accelerator reaction, which otherwise would overlap with the heat released during the initial mixing of cement and water [12].

For isothermal calorimetry, 100 g of paste were prepared and 8.00 g of the amount produced were transferred with a spatula

to a glass flask, which was consolidated for 5 s to eliminate entrapped air. Immediately after consolidation, the flask was sealed and put inside the calorimeter to start the readings. For the determination of setting times, 300 g of paste were prepared. The mold used for the test was filled with the paste and consolidated. The remaining amount was destined to XRD. 4 plastic flasks were filled with 8.00 g of paste, sealed and stored at 23 °C until the time to stop hydration. The molding operations in all the cases lasted 1 min, in order to start the tests as early as possible.

2.2.2. Concrete

The mix composition of the concrete matrix is presented in Table 6. The cementitious material was composed by 70% CEM I 52.5R and 30% of blast-furnace slag.

One batch containing 5 m^3 of concrete was produced and used to spray 5 different mixes (REF, AF 6%, AF 8%, AK 2% and AK 4%). This quantity was necessary to comply with the requirements of the spraying equipment, to assure a homogeneous flow of matrix through the pumping system and to provide enough material to fill up all the panels destined to the mechanical tests. The mixing process was performed in a concrete truck mixer with the capacity of 8 m^3.

Fine sand, coarse sand and gravel were added to the mixer and homogenized for 300 s. Then, cement was added and mixed for 300 s, followed by water addition and an additional mixing for 300 s. Finally, plasticizer, superplasticizer and retarder were added separately and homogenized for 180 s in each step. The fresh concrete showed adequate workability for pumping and spraying (slump equal to 180 mm [22], with no bleeding nor segregation). It presented a specific weight equal to 2.33 kg/m^3 [23] and its air content was 1.5% [24]. Once the mixing process was finished, concrete was transported to the worksite, where it was sprayed with accelerators 1 h after cement and water had been mixed.

2.3. Concrete spraying process

The spraying process was conducted outdoors due to the logistics of the process. The temperature during the first 24 h after spraying varied between 17 and 25 °C. A Brazilian rotor type pump CP10 SU coupled with an air compressor with the maximum pressure of 28 bar was employed to spray concrete. This type of pump is adequate for fluids containing coarse particles, such as fresh concrete [25]. The concrete flow was kept constant at 8 m^3/h, with a minimum pulsation effect. It is important to mention that the spraying operation was conducted by specialized professionals and nozzleman. Fig. 4 shows the execution of the spraying process.

Accelerators were dosed by an air-operated diaphragm pump type E-300. This type of pump presented a homogeneous suction for both accelerators, since their viscosity varied according to their chemical composition. The flow of accelerators depended on their type and dosage and was calculated based on the optimal flow of concrete.

The hose for transporting the fresh concrete measured 30 m in length and 76.2 mm in inner diameter. A frustum-shaped nozzle, with base diameter, top diameter and height equal to 80.0, 50.0 and 300.0 mm, was connected at the exit of the hose. The nozzle contained two different inlets for the ingress of concrete and accelerator. Square frustum-shaped wood panels were designed according to [26]. Their base side, top side and height measured 1000, 600 and 200 mm, respectively. One panel was used for each mixture (REF, AF 6%, AF 8%, AK 2% and AK 4%) to obtain specimens for the mechanical tests.

During the spraying operation, the distance between the exit of the nozzle and the wood panels was kept equal to 1.0 m and concrete was sprayed perpendicularly to the bottom of the panel, following the procedures from [27]. After spraying, panels were covered with a plastic sheet and demolded 23 h later. Finally, cores were extracted, cut and polished and destined to the compression test at the age of 24 h or to the curing in a humid chamber for compression tests at the ages of 28 and 91 days.

Table 6
Mix composition of concrete.

Material	Dosage (kg/m^3)	Relative amount
Cementitious material	400.0	1.00
Fine sand (0–1.2 mm)	574.0	1.44
Coarse sand (0–4.75 mm)	315.0	0.788
Gravel (4.75–12.5 mm)	840.0	2.10
Water	200.0	0.50
Plasticizer	1.84	0.0046
Superplasticizer	0.84	0.0021
Retarder	1.12	0.0028

2.4. Test methods

Table 7 summarizes the tests performed with cement pastes and concretes. Their descriptions are presented in Sections 2.4.1 and 2.4.2. Accelerator addition was considered as the beginning (time 0) for all the tests. Isothermal calorimetry, determination of setting times and evolution of temperature started 2 min after accelerator addition.

2.4.1. Cement pastes

2.4.1.1. Isothermal calorimetry. Isothermal calorimetry was performed at 23 °C during 24 h with 8.0 g of cement paste, using a TAMAir isothermal calorimeter. This test was performed to analyze the hydration behavior of cement pastes containing different blast-furnace slag contents in order to select the most adequate cement substitution percentage for the execution of the other tests described in this study.

2.4.1.2. Powder X-ray diffraction. Powder XRD was conducted in a PANalytical X'Pert PRO MPD Alpha1 powder diffractometer in reflection Bragg-Brentano θ/2θ geometry equipped with an X'Celerator detector (active length of 2.122°) and a fixed divergence slit of 0.5°. It operates with Ni-filtered CuKα radiation (λ = 1.5418 Å) at 45 kV and 40 mA. Sample holders were cylindrical, with a diameter of 16 mm and a depth of 2.5 mm. They were backloaded and spun at 2 revolutions per second.

Diffraction patterns were recorded from 5 °2θ to 70 °2θ, using a step width of 0.017 °2θ and 100 s per step. They were analyzed quantitatively by Rietveld refinement using the software X'Pert HighScore Plus with the structure models shown in Table 8. Amorphous content was determined by the external standard method [18] to provide an indirect assessment of the C—S—H amount contained in the matrix using alumina powder (SRM 676a, from NIST) as a standard reference material.

Hydration was stopped by solvent exchange at 15 min, 3 h, 12 h and 24 h after accelerator addition. This method was employed because it does not affect the stability and crystallinity of hydrated aluminate phases, as indicated by [44]. The procedure consisted in six steps: Firstly, the paste was immersed in isopropanol (solvent/paste ratio equal to 10) for 1 h at −4 °C. Secondly, solvent was replaced by a new volume of isopropanol (solvent/paste ratio equal to 10) and the paste was kept immersed for 1 h at −4 °C. Thirdly, solvent was replaced by a new volume of isopropanol (solvent/paste ratio equal to 50) and immersion occurred for 24 h at −4 °C. Fourtly, isopropanol was replaced by diethyl ether (solvent/paste ratio equal to 25) and the paste was kept immersed for 24 h at −4 °C. Then, solvent was removed and the sample was dried for 30 min at 40 °C. Finally, the paste was crushed and ground to a maximum size of 63 μm in an agate mortar.

Fig. 4. Spraying process: organization of the process (a and b), concrete spraying process conducted by specialized nozzleman (c). Description of equipment: concrete spraying machine and accelerator pump (1), concrete mixer (2), air compressor (3), hose for accelerators (4), hose for concrete (5), nozzle (6), panels (7).

Table 7
Tests performed with cement pastes and concretes.

Matrix	Test	Specimen	Age/period	Reference
Cement paste	Isothermal calorimetry	Paste in fresh state	0–24 h	[28]
	Powder XRD	Ground hardened paste	15 min, 3 h, 12 h, 24 h	[10]
	Determination of setting times	Paste in fresh state	0 - final setting	[29]
Sprayed concrete	Evolution of temperature	Concrete panels	1–23 h	[7]
	Needle penetration test	Concrete panels	10, 20, 30, 40, 50, 60 min	[30]
	Compressive strength	Extracted cores	24 h, 28 days, 91 days	[31]

2.4.1.3. Determination of setting times. Setting times were determined using a Vicat penetrometer. Although the standard UNE EN 196-3 (2009) [29] prescribes the use of a normal consistency paste, a w/cm equal to 0.45 was adopted to facilitate handling and molding of the accelerated pastes and because it generates enough space for proper cement hydration and crystal growth [19]. Moreover, when low w/cm ratios are used (0.27–0.32, for example), initial setting occurs approximately 2 min after accelerator addition, even when superplasticizers are used [45]. This would make the paste unworkable before the mold was filled, leading to inaccuracies in the results.

2.4.2. Sprayed concrete

2.4.2.1. Evolution of temperature. Evolution of temperature was measured directly in the sprayed panels. Two LM 35 sensors (precision equal to 0.1 °C) were positioned at the center of the bottom face of each panel. This test started right after accelerator addition and was performed for 23 h, configuring a data acquisition frequency equal to one point per minute.

2.4.2.2. Needle penetration test. Needle penetration test was performed to determine an indirect compressive strength of sprayed concrete until 60 min after accelerator addition. The procedure

Table 8
References of the different phase structures used for Rietveld refinement.

Phase	Formula	Crystal system	PDF number	ICSD code	Reference	Year
Alite	Ca_3SiO_5	Monoclinic	01-070-8632	94742	[32]	2002
Belite	Ca_2SiO_4	Monoclinic (β)	01-083-0460	79550	[33]	1994
Calcium aluminate	$Ca_3Al_2O_6$	Cubic	00-038-1429	1841	[34]	1975
Ferrite	Ca_2AlFeO_5	Orthorhombic	01-071-0667	9197	[35]	1971
Gypsum	$CaSO_4{\cdot}2H_2O$	Monoclinic	00-033-0311	151692	[36]	2004
Calcite	$CaCO_3$	Rhombohedral	01-083-0577	79673	[37]	1989
Portlandite	$Ca(OH)_2$	Rhombohedral	01-072-0156	15741	[38]	1961
Ettringite	$Ca_6Al_2(SO_4)_3.(OH)_{12}{\cdot}26H_2O$	Hexagonal	00-041-1451	155395	[39]	2006
Monosulfoaluminate	$3CaO.Al_2O_3.CaSO_4{\cdot}12H_2O$	Rhombohedral	–	24461	[40]	1968
Hemicarboaluminate	$Ca_4Al_2(OH)_{12}.OH.0.5CO_3{\cdot}4H_2O$	Rhombohedral	00-041-0221	263124	[41]	2012
Monocarboaluminate	$Ca_4Al_2(OH)_{12}.CO_3{\cdot}5H_2O$	Triclinic	01-087-0493	59327	[42]	1998
Alumina (standard)	Al_2O_3	Rhombohedral	01-081-2267	73725	[43]	1993

[30] consists in introducing a cylindrical needle mechanically into the matrix until the penetration of 25 mm is reached. The diameters of the needles were 4.5, 6.4 and 9.0 mm and each needle was chosen according to matrix strength, so that the minimum penetration force at 25 mm was 100 N. The resulting force was converted into compressive strength using the calibration curve provided in [26]. Five penetrations were performed at each age (10, 20, 30, 40, 50 and 60 min).

2.4.2.3. Compressive strength. Compressive strength was determined from direct compression tests performed in cylindrical concrete cores measuring 75 mm in diameter and 150 mm in length extracted from sprayed panels. Tests were conducted in a Shimadzu Universal Testing Machine, model UH-F1000 kN, at a loading rate equal to 0.45 MPa/min, according to [31]. Four specimens were tested at each age (24 h, 28 days and 91 days).

3. Results and discussion

Results obtained with cement pastes and sprayed concrete are presented in Sections 3.1 and 3.2, respectively.

3.1. Cement pastes

3.1.1. Isothermal calorimetry

Fig. 5 shows the heat flow curves of accelerated cement pastes from 0 to 24 h. Fig. 5.a, 5.b, 5.c and 5.d represent the pastes with 0%, 15%, 30% and 45% of blast-furnace slag, respectively. The period from 1.0 to 1.5 h covers the exothermic signal generated by accelerator addition and is named accelerator peak hereinafter. Table 9 summarizes the characteristic points of the heat flow curves, determined according to [46]. The conclusions derived from this analysis are presented subsequently.

A clear influence of the blast-furnace slag on the hydration behavior of the REF cement pastes (without accelerator) is observed. As the amount of slag increases, induction periods become longer, indicating that this addition retards the onset of cement hydration. In addition, the main hydration peak broadens, achieving lower values of energy released and maximum intensities. The degree of hydration at 24 h is also lower for increasing amounts of slag. As expected, the addition of slag promoted decreases in the overall hydration rate, because slag is less reactive than the minerals present in cement [13]. It is important to mention that REF pastes present a retarding effect caused by the superplasticizer.

Blast-furnace slag also influences accelerator reaction, as observed in the analysis of the accelerator peak. Reaction rate, energy released and maximum heat flow decrease as the slag content increases. This reduction is more significant when accelerator AK is employed, because this accelerator does not contain sulfates in its formulation and the replacement of cement by slag reduces the overall sulfate content in the paste. Since accelerator reactivity is proportional to the gypsum content in cement [46], accelerator AK is less reactive than accelerator AF in cement pastes produced with slag.

All accelerated pastes evaluated present shorter induction periods than the respective REF pastes and this reduction is a function of accelerator type and dosage, as expected [46]. The duration of the induction period is proportional to the amount of slag employed in each paste. As slags present lower reactivity than clinker minerals, the onset of the main hydration peak is postponed, as discussed in the analysis of REF pastes.

Reaction rates in the main hydration peak of the accelerated pastes tend to decrease when slag is added. Energy released, maximum heat flow and degree of hydration in all accelerated pastes are reduced proportionally to the amount of slag employed. Such reduction is more evident when AK accelerator is used, because the early formation of AFm phases due to undersulfated C_3A reaction inhibits alite hydration [28,46].

In order to deepen the analysis on the influence of slag on the hydration behavior of accelerated cement pastes, theoretical heat flow curves were calculated based on the curve of each paste produced with 100% CEM I (no slag). The experimental values were multiplied by 0.85, 0.70 and 0.55 to obtain the heat flow curve derived from the cement amount in pastes containing 15%, 30% and 45% of slag, respectively. By doing so, the theoretical heat flow values of cement pastes containing 15%, 30% and 45% of inert material substituting cement may be inferred. The comparison of the experimental and theoretical heat flow curves is presented in Fig. 6 for REF pastes and in Fig. 7 for accelerated pastes. Different graphs were plotted in order to provide a proper scale for each analysis.

Analyzing the REF pastes (Fig. 6), it is possible to observe that the experimental curves present longer induction periods than the respective theoretical ones. It may be inferred that the superplasticizer also retards slag hydration. Although the hydration rate (slope of the ascending part of the curve) is similar for both curves, higher values of maximum heat flow are obtained in the experimental curves. This means that slag hydration contributes to generate heat during the main hydration peak.

As depicted in Fig. 5, a very distinct behavior is observed when accelerators are employed. The experimental curves (dotted lines) present shorter induction periods, higher hydration rates and higher values of maximum heat flow in the main hydration peak, when compared to the respective theoretical curves. In pastes produced with AK 4%, a sharp peak is observed between 1.5 and 3 h in the experimental curves, due to accelerated C_3A hydration [46]. That peak is not observed in the theoretical curves, because they are derived from a properly-sulfated paste [46].

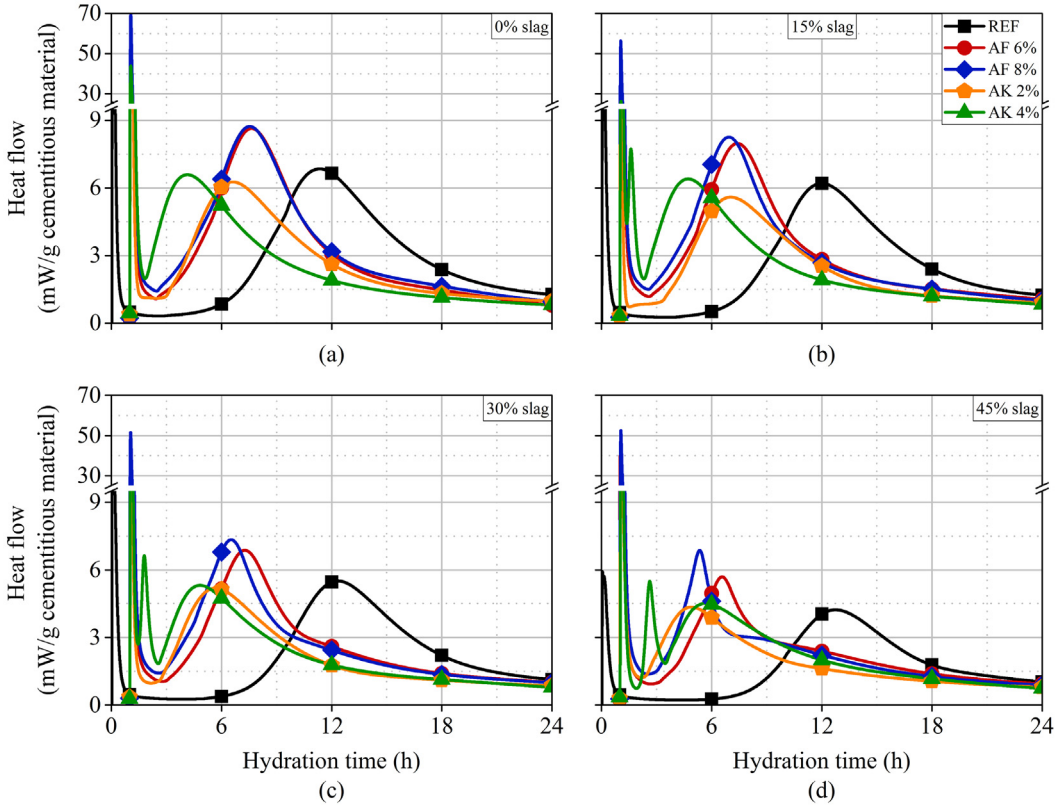

Fig. 5. Heat flow curves from 0 to 24 h obtained with cement pastes produced with CEM I 52.5R and different amounts of blast-furnace slag: 0% (a), 15% (b), 30% (c) and 45% (d).

Table 9
Analysis of the heat flow curves obtained with the cement pastes.

Sample	Slope - accelerator peak (mW/g.h)	Energy released - accelerator peak[a] (J/g)	Maximum heat flow - accelerator peak (mW/g)	Induction period (h)	Slope acceleration - main peak (mW/g.h)	Energy released - main peak[b] (J/g)	Maximum heat flow – main peak (mW/g)	Energy released until 24 h[c] (J/g)
0% slag_REF	–	–	–	6.2	1.55	239.0	6.85	242.2
0% slag_AF 6%	2341	30.3	56.0	1.0	2.29	233.5	8.65	262.8
0% slag_AF 8%	2878	38.2	70.0	0.8	2.22	254.2	8.73	280.1
0% slag_AK 2%	1354	17.2	32.4	0.9	1.96	203.6	6.26	228.4
0% slag_AK 4%	1805	29.7	43.9	0.0	3.10	199.0	6.59	221.8
15% slag_REF	–	–	–	6.5	1.44	212.6	6.20	214.6
15% slag_AF 6%	1371	22.4	36.2	1.7	2.22	227.8	7.98	251.6
15% slag_AF 8%	2407	32.7	56.4	1.3	2.36	229.7	8.26	251.0
15% slag_AK 2%	628	7.7	14.9	1.5	1.07	174.3	5.59	196.8
15% slag_AK 4%	1053	18.5	26.2	0.0	2.58	199.4	6.40	221.4
30% slag_REF	–	–	–	7.2	1.38	177.4	5.51	191.0
30% slag_AF 6%	1456	22.0	36.4	1.8	1.86	198.2	6.87	223.0
30% slag_AF 8%	2159	30.1	51.5	1.4	2.09	199.5	7.34	216.8
30% slag_AK 2%	618	10.4	15.9	0.7	1.92	154.6	5.18	181.4
30% slag_AK 4%	740	14.3	19.9	0.0	2.23	171.3	5.31	198.5
45% slag_REF	–	–	–	7.7	1.08	131.3	4.22	144.9
45% slag_AF 6%	2175	25.0	45.1	1.6	1.74	164.0	5.69	184.6
45% slag_AF 8%	2271	31.8	52.4	1.2	3.14	160.7	6.86	186.8
45% slag_AK 2%	602	13.0	16.0	0.7	1.66	130.9	4.35	163.3
45% slag_AK 4%	810	14.4	19.5	0.4	1.70	157.4	4.49	188.2

[a] The area under the curve was calculated from 1.0 to 1.5 h.
[b] The area under the main hydration peak was calculated from the end of the induction period until the time when the heat flow reached 1.0 mW/g of cement in the deceleration period.
[c] Calculated by the total energy released until 24 h minus the energy released in the accelerator peak, in order to evaluate the energy associated with cement hydration.

This approach indicates that slag is activated when all accelerators are used, especially in pastes containing the alkaline accelerator because the sodium hydroxide in its formulation facilitates slag hydration [47]. Although the degree of hydration in pastes containing slag is lower than in pastes composed by 100% CEM I, a proper hydration behavior is observed (maximum heat flow

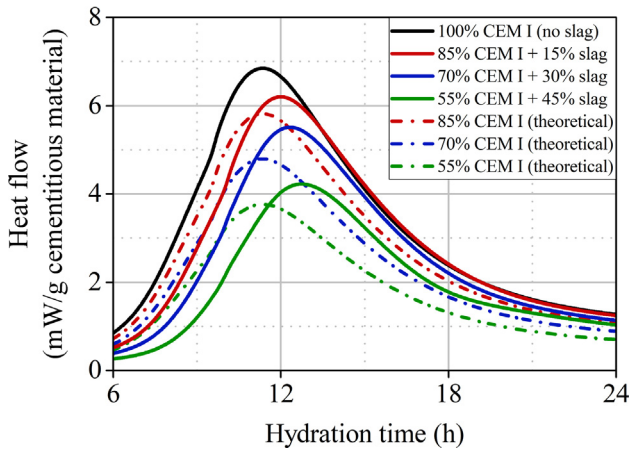

Fig. 6. Experimental and theoretical heat flow curves from 6 to 24 h obtained with REF cement pastes (no slag).

above 4 mW/g of cementitious material, according to [10]). Therefore, it may not be detrimental for the evolution of mechanical strength of sprayed concrete produced with accelerators.

3.1.2. Powder XRD

Fig. 8 presents the quantitative evolution of phase composition determined with all cement pastes from 0 to 24 h. In order to simplify the interpretation of the graphs, only the reacting phases (alite, portlandite, gypsum, ettringite and AFm) are presented. Slow reacting phases (belite and ferrite) were not plotted. The amorphous content was corrected considering the slag amount added to the paste.

The REF paste presents a slow hydration rate until 12 h, due to the addition of the superplasticizer. At 12 h, alite consumption is noticed, with the formation of small amounts of portlandite and amorphous phases. Ettringite starts to precipitate at 12 h, with consequent consumption of calcium sulfate. Gypsum depletes between 12 and 24 h and no AFm phases were detected within the first 24 h.

All accelerated pastes present a significant precipitation of ettringite due to accelerator reaction (initial value in the graphs in Fig. 8.a). Ettringite formation increases the solid/liquid ratio of the matrix [48], interconnects the solid phase and leads to reduction in porosities [10]. The amount of ettringite formed follows the ascending order of the Al^{3+} content in alkali-free accelerators (REF < AF 6% < AF 8%). Therefore, shorter setting times and faster rates of early strength development may be obtained with accelerators containing larger Al^{3+} amounts.

Initial ettringite formation is associated with gypsum consumption, as observed in Fig. 8.b. When accelerator AF is used, gypsum remains after accelerator reaction, which may control further C_3A hydration. This may be observed by the constant ettringite formation until 12 h for AF 6% and until 8 h for AF 8%. However, when AK is employed, gypsum depletes instantly, because this accelerator does not contain sulfates in its composition (Table 4). This leads to undersulfated accelerated C_3A reactions, consuming ettringite and forming AFm phases from 6 h on in paste AK 2% (Fig. 8.c).

Ettringite contents in paste AK 4% were smaller than expected, as this accelerator contains an average Al^{3+} concentration, within the contents in AF 6% and AF 8%. This occurs because accelerator AK has no sulfate in its composition, which leads to the formation of AFm phases right after accelerator addition, as observed in Fig. 8.c. The formation of AFm phases also contributes to increase the solid-liquid ratio of the matrix and to reduce setting times [49].

Alite is slowly consumed until approximately 3 h in all accelerated pastes (Fig. 8.d) to balance the concentration of Ca^{2+} in the liquid phase, initially disturbed by accelerators [31]. From 3 h on, the rate of alite hydration increases, with consequent formation of portlandite (Fig. 8.e) and amorphous phases (Fig. 8.f).

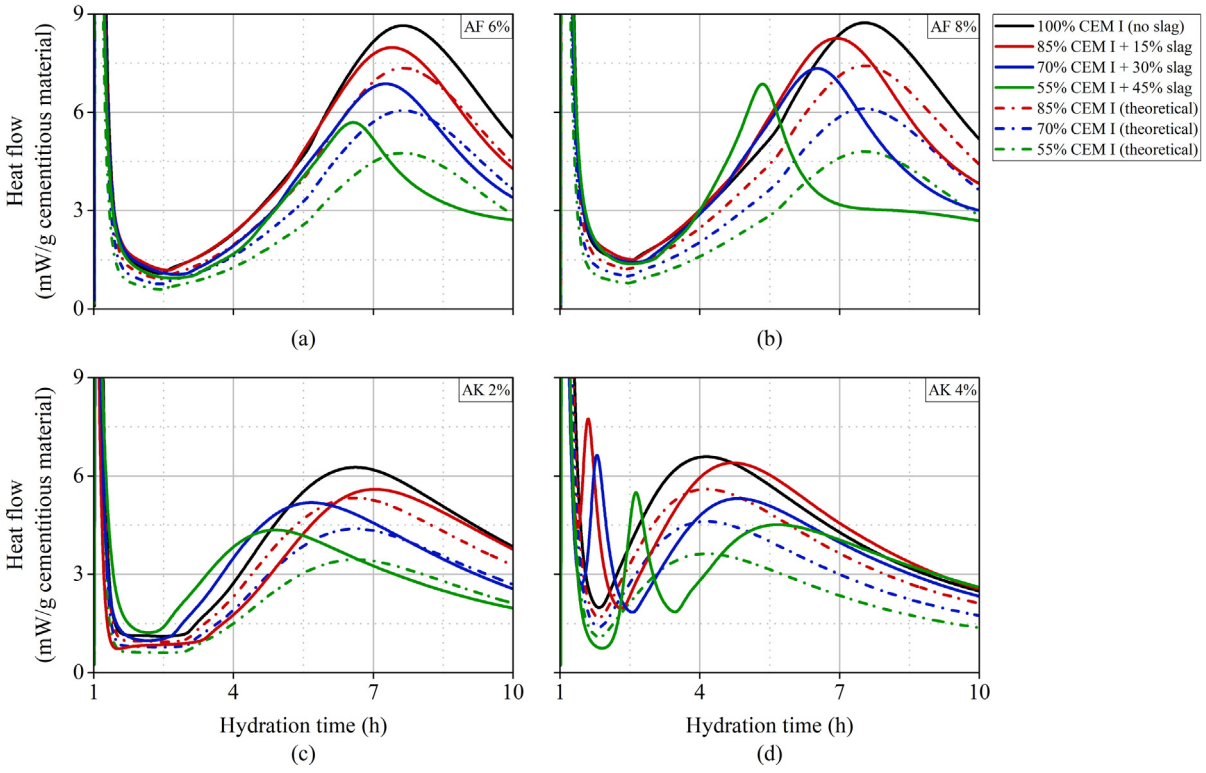

Fig. 7. Experimental and theoretical heat flow curves from 1 to 10 h obtained with accelerated cement pastes: AF 6% (a), AF 8% (b), AK 2% (c) and AK 4% (d).

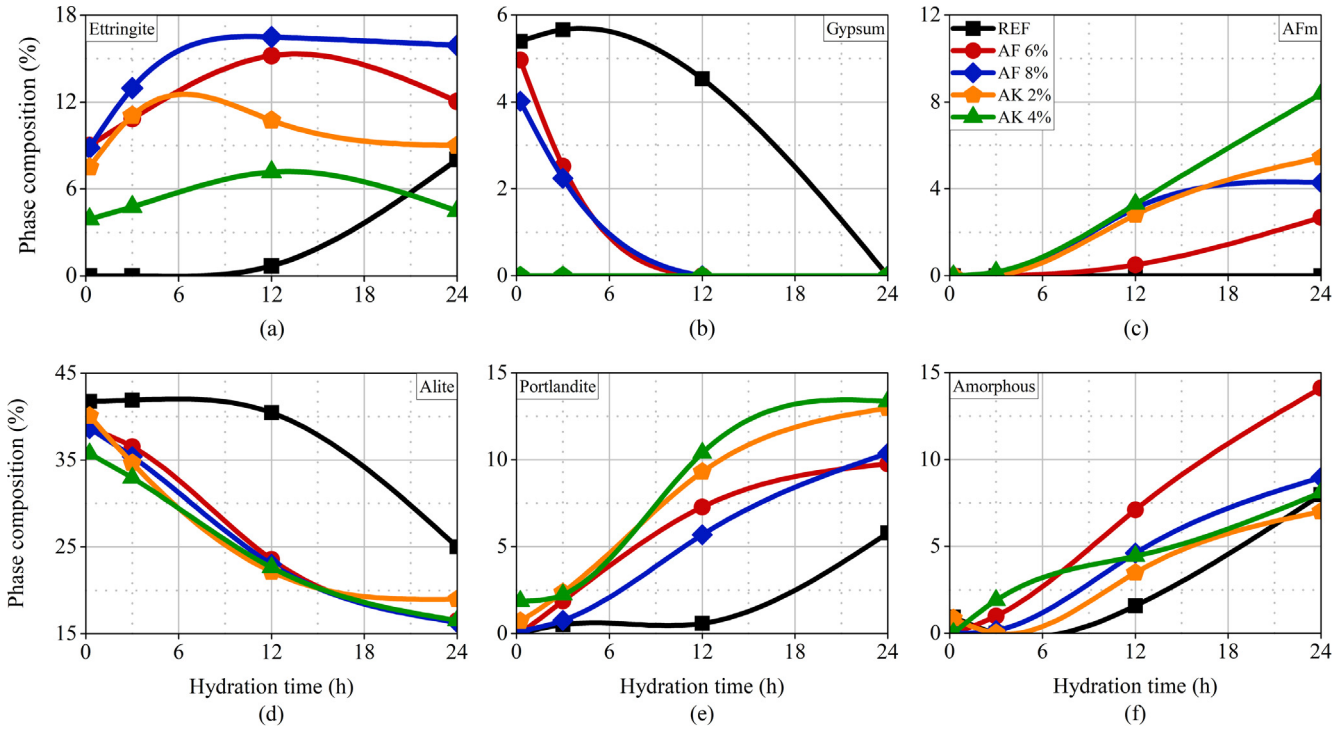

Fig. 8. Evolution of ettringite (a), gypsum (b), AFm phases (c), alite (d), portlandite (e) and amorphous phases (f) contents obtained with cement pastes produced with CEM I 52.5R and 30% of blast-furnace slag.

Initial alite dissolution in pastes AK 2% and AK 4% is favored because this accelerator contains NaOH, which leads to a faster portlandite precipitation [50]. However, since gypsum is depleted right after accelerator addition, undersulfated accelerated C_3A hydration takes place before the onset of silicate acceleration period. This process delays alite hydration from 12 h on due to the space filling caused by the early formation of aluminate hydrates and to the precipitation of these phases on the surface of alite, reducing its solubility.

Comparing these results (pastes produced with 70% CEM I + 30% blast-furnace slag) with XRD results from [28] (pastes produced with 100% CEM I), alite consumption and portlandite formation from accelerator addition until 24 h are around 15% lower when slag is employed with alkali-free accelerators and 7% lower in the case of alkaline accelerators. Although the degree of hydration until 24 h is lower, these values are above the substitution of 30% of CEM I by slag. Therefore, slag does not influence the evolution of the hydration process negatively from 3 h on when accelerators are added because it may be activated. Therefore, slag may be employed in sprayed concrete applications, especially when the alkaline accelerator is used at 2% bcmw.

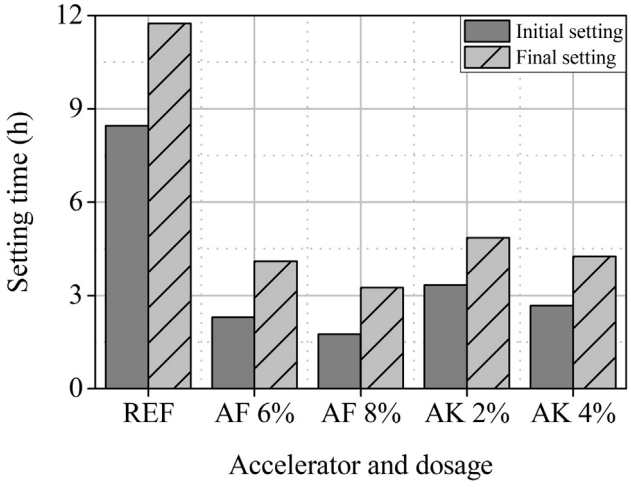

Fig. 9. Setting times determined with cement pastes produced with CEM I 52.5R and 30% of blast-furnace slag.

3.1.3. Determination of setting times

Fig. 9 presents setting times determined with cement pastes produced with CEM I 52.5 R and 30% of blast-furnace slag. Results obtained vary considerably in pastes with and without accelerators. Cement and slag hydration in reference pastes are significantly retarded by the superplasticizer, increasing setting times.

Setting times are reduced in accelerated pastes and depend on accelerator type and dosage. Pastes produced with accelerator AF present shorter setting times than pastes containing AK. As observed in XRD (Section 3.1.2), the amount of ettringite and AFm phases formed in accelerated pastes depends on the Al^{3+} concentration in accelerators (the higher the Al^{3+} content, the shorter the setting time). Since ettringite and AFm phases are the main products that lead to initial mechanical strength in the matrices evaluated, the larger the amount of these compounds formed by accelerator reaction, the shorter the setting times of the pastes. Therefore, the ascending order of setting times is REF > AK 2% > AK 4% > AF 6% > AF 8%. This evaluation is in total agreement with the isothermal calorimetry results (Section 3.1.1).

3.2. Sprayed concrete

3.2.1. Evolution of temperature

Fig. 10 shows the evolution of temperature curves obtained in sprayed concrete panels from accelerator addition until 23 h. The

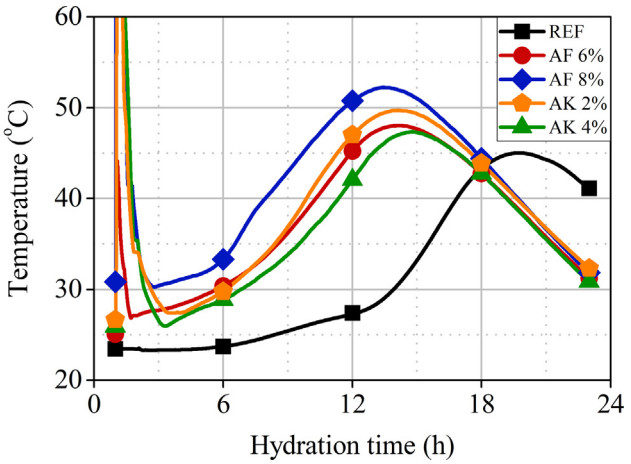

Fig. 10. Evolution of temperature obtained with sprayed concrete produced with CEM I 52.5R and 30% of blast-furnace slag from accelerator addition until 23 h.

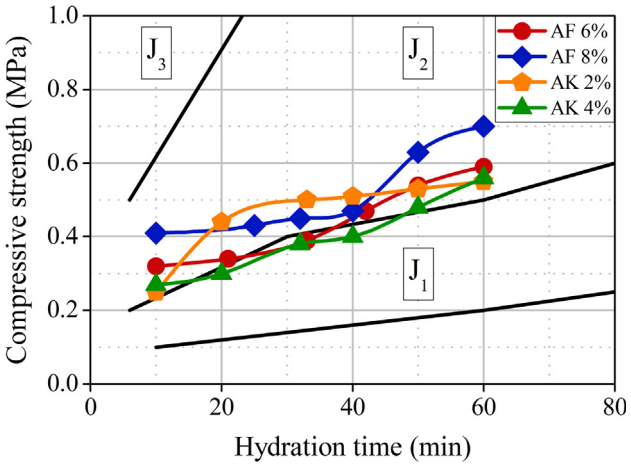

Fig. 12. Average values of indirect compressive strength obtained by needle penetration in sprayed concrete produced with CEM I 52.5R and 30% of blast-furnace slag from 10 to 60 min after accelerator addition.

REF concrete presents the slowest hydration rates, when compared to the other matrices. Faster hydration kinetics are observed when accelerators are employed, as expected.

Concrete AF 8% presents the shortest induction period and the highest intensity in the main hydration peak. These results are in line with the heat flow curves obtained by isothermal calorimetry (Section 3.1.1) and with the XRD results (Section 3.1.2). Concrete AK 4% behaves in the opposite manner, that is, induction period is the longest and intensity in the main hydration peak is the lowest. This occurs because spraying enhances accelerator reactivity and leads to the formation of AFm phases at the moment of accelerator addition, which decreases the extent of alite hydration and the generation of heat during the main hydration peak [12].

In order to provide an indirect assessment of compressive strength until 23 h, the evolution of temperature curve was integrated using the Nurse-Saul function [9,51]. The curves obtained are presented in Fig. 11. All the curves present a continuous increase in the integrated values until 23 h, indicating that the evolution of mechanical properties is continuous in the period analyzed. In addition, it is possible to observe the influence of accelerator type on strength development until 23 h. Accelerator AK 8% provided the highest integrated value, indicating this matrix may present the highest compressive strength at 23 h. This discussion is in accordance with [9].

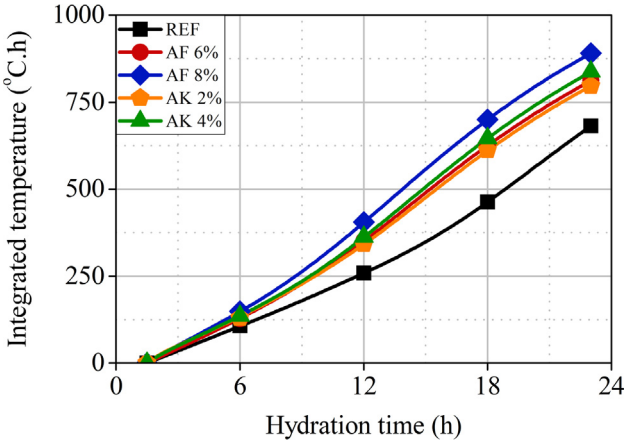

Fig. 11. Integration of the evolution of temperature curve obtained with sprayed concrete produced with CEM I 52.5R and 30% of blast-furnace slag from accelerator addition until 23 h.

3.2.2. Needle penetration resistance

Fig. 12 presents the average results of indirect compressive strength determined by needle penetration from 10 to 60 min after accelerator addition in sprayed concrete. In order to facilitate the analysis, the curves of mechanical strength development J_1, J_2 and J_3 [6,26] were also plotted in the same figure. Reference concrete (without accelerator) was not evaluated because this period covers the induction period in this sample and no evolution of detectable penetration resistance was observed.

The initial mechanical strength depends on accelerator type and dosage. The matrix produced with AK 8% (alkali-free accelerator at the highest dosage) presents the highest initial compressive strength, an all the values measured in the time interval are above the J_2 minimum limit. This occurs because this accelerator provides the highest Al^{3+} amount to the matrix. This fact corroborates the results obtained by isothermal calorimetry, powder XRD and setting times in cement pastes (Sections 3.1.1, 3.1.2 and 3.1.3, respectively), as the amount of ettringite formed by accelerator reaction is the responsible for initial strength development.

The evolution of compressive strength in sprayed concrete depends on the rate of ettringite formation from 15 min to 3 h determined by powder XRD. As observed in Fig. 8, the rate of ettringite formation in paste AK 4% is the lowest due to the limited sulfate content in the matrix. Therefore, initial mechanical strength evolution occurs at the lowest rate. This occurs because when slag is used to replace cement, gypsum amount in the matrix is reduced, which decreases accelerator reactivity and the penetration resistance consequently [46].

As observed in isothermal calorimetry (Section 3.1.1) and XRD results (Section 3.1.2), the accelerators employed activate slag hydration. Therefore, blast-furnace slag does not compromise the mechanical strength development of the matrix, which may fulfil the requirements of compressive strength at early ages if the classes J_1 or J_2 are specified.

3.2.3. Compressive strength

Fig. 13 shows the results of compressive strength at the age of 24 h, determined with cores extracted from sprayed concrete panels. In order to facilitate the analysis, the values of compressive strength from sprayed concrete classified as J_1, J_2 and J_3 [6,26] were also plotted in the same figure. Fig. 14 presents the results of compressive strength at 28 and 91 days.

A significant difference in the results of reference and accelerated concretes is observed. The REF matrix shows the highest val-

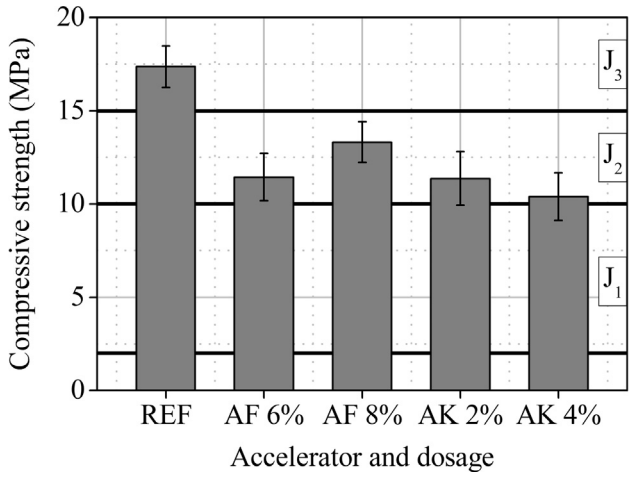

Fig. 13. Compressive strength at 24 h obtained with sprayed concrete produced with CEM I 52.5R and 30% of blast-furnace slag.

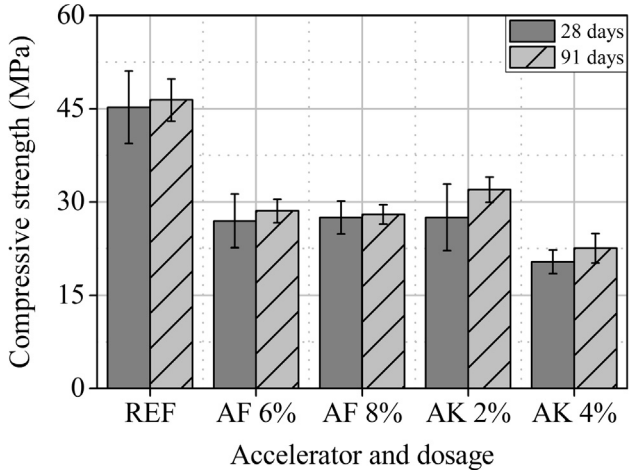

Fig. 14. Compressive strength at 28 and 91 days obtained with sprayed concrete produced with CEM I 52.5R and 30% of blast-furnace slag.

ues of compressive strength in all ages analyzed. Concretes sprayed with accelerators present lower values of compressive strength due to the fast setting caused by accelerators. The fast setting leads to higher porosities, because the matrix does not consolidate properly and does not eliminate the air entrapped during spraying. Since compressive strength is inversely proportional to porosity, the use of accelerators tends to decrease the mechanical strength of matrix. This discussion is in accordance with the results presented in [1,10,50].

In addition to the higher values of water accessible in sprayed concrete, reductions in compressive strength may be caused by the use of slag and retarder in the production of concrete. Although slag may be activated by the accelerators, its hydration is slower when compared to clinker minerals (Fig. 5). As commented in section 2.1, the use of the retarder may cause a reduction in the early strength development due to slow down in the building up of the supersaturation needed for the nucleation of hydrates, delaying the formation of C—S—H [20].

At the age of 1 day, the values of compressive strength of sprayed concrete containing accelerators are between 10 and 15 MPa. The values obtained are above the minimum compressive strength specified for a sprayed concrete from the J_2 class at 24 h. At this age, compressive strength is directly proportional to the rate of cement hydration, that is, to the evolution of temperature of the matrix. Therefore, the ascending order of compressive strength in sprayed concrete containing accelerators is AF 8% > AF 6% > AK 2% > AK 4%. The highest compressive strength is obtained when AF 8% is employed, because this accelerator and dosage provide the highest rate of cement hydration, as observed in Figs. 5 and 10. The lowest compressive strength is observed when AK 4% is used because the early formation of AFm phases by accelerator reaction and by undersulfated C_3A hydration inhibits further alite hydration [28].

Compressive strength at later ages fall within the interval from 25 to 35 MPa. The ascending order of compressive strength in sprayed concrete containing accelerators is AK 2% > AF 6% > AF 8% > AK 4%. The highest value of compressive strength at 28 and 91 days is obtained when the lowest amount of accelerator is employed (AK 2%). This happens because when low dosages of accelerator are used, the setting time of the matrix is longer, as observed in Fig. 9, which shows that paste AK 2% presents the longest setting times. Therefore, sprayed concrete may consolidate better than when higher dosages are employed, leading to higher compressive strength.

Results obtained at 24 h 28 days are similar to the ones presented by [1], who employed CEM II/A-L containing 13% of limestone filler in substitution of cement to produce sprayed concrete. This indicates that blast-furnace slag may be employed for sprayed concrete applications, when the J_2 class is specified.

4. Conclusions

The following conclusions may be drawn according to the results obtained from the experimental program conducted:

- All cement pastes containing blast-furnace slag present slower hydration kinetics than CEM I pastes at early ages. Accelerator reactivity is lower, induction periods are longer, the main hydration peak is broader and the degree of hydration at 24 h is lower when slag is employed because this addition is less reactive than the minerals present in cement. These reductions depend on the slag content in the matrix (the higher the slag content, the less reactive the paste). However, slag is activated by the accelerators used for sprayed concrete and the matrix may achieve a proper hydration behavior for strength development (intensity in the main hydration peak above 4.0 mW/g of cementitious material).
- Blast-furnace slag does not influence the evolution of the hydration process negatively from 3 h on when accelerators are added. Alite consumption and portlandite formation until 24 h are around 7–15% lower when slag is employed. These reductions are below the slag substitution percentage, which was equal to 30%.
- Compressive strength until 60 min determined by penetration resistance is reduced when slag is used to replace cement. This occurs because the gypsum amount in the matrix is also reduced, decreasing accelerator reactivity and, consequently, the initial mechanical strength of the matrix.
- Compressive strength of sprayed concrete containing 30% of blast-furnace slag at 24 h and 28 days are similar to the values obtained when CEM II/A-L containing 13% of limestone filler is employed. Slag hydration contributes to increase the mechanical strength of the matrix, although its evolution occurs at low rates.
- The strength values from 10 to 60 min determined by penetration resistance and at 24 h determined by compressive strength of extracted cores are above the minimum values specified for a sprayed concrete from the J_2 class.

- Further studies are required in order to provide a mix composition containing slag capable to achieve the J_3 class. As a recommendation to increase slag reactivity and improve the mechanical strength development, the use of accelerators with higher compatibility with blast-furnace slag, such as formulations containing high contents of alkaline hydroxides, may be a feasible option.

Declaration of Competing Interest

None.

Acknowledgements

This research was partially supported by the Laboratory of Microstructure and Eco-efficiency of Materials (LME) and INCT (grant#2014/50948-3, São Paulo Research Foundation (FAPESP)). The first author would like to thank FAPESP (Fundação de Amparo à Pesquisa do Estado de São Paulo, São Paulo, Brazil, process 2017/00125-9) for the scholarship granted. The authors thank São Judas Tadeu University for financial support. Thanks are extended to Solotrat and Concreto Projetado do Brasil for lending equipment and offering technical support, Sika Brazil for providing admixtures and Lafarge-Holcim for providing concrete.

Appendix A. Supplementary data

Supplementary data to this article can be found online at https://doi.org/10.1016/j.conbuildmat.2019.05.132.

References

[1] I. Galobardes, Characterization and control of wet-mix sprayed concrete with accelerators. Ph.D. Thesis (2013).
[2] M. Jolin, D. Beaupré, Understanding wet-mix shotcrete: mix design, specifications, and placement, Shotcrete Mag. Summer 2003, Am. Shotcrete Assoc. (2003).
[3] http://www.marketsandmarkets.com/Market-Reports/Sprayed-concrete-shotcrete-market-1116.html, Shotcrete/Sprayed Concr. Mark. by Process (Wet - Mix Dry - Mix. by Appl. (Undergr. Constr. Water Retaining Struct. Prot. Coatings, Repair Work. Others), by Syst. (Robotic Manual) by Reg. - Glob. Trends Forecast. (2015) 243. http://www.marketsandmarkets.com/Market-Reports/Sprayed-concrete-shotcrete-market-1116.html (accessed December 12th, 2018).
[4] N. Ginouse, M. Jolin, Mechanisms of placement in sprayed concrete, Tunn. Undergr. Sp. Technol. 58 (2016) 177–185, https://doi.org/10.1016/j.tust.2016.05.005.
[5] A. Thomas, Sprayed Concrete Lined Tunnels, CRC Press (2008), https://doi.org/10.1201/9781482265682.
[6] Austrian Building Technology Association (ÖBV), Guidelines: Sprayed Concrete, Vienna, 2013.
[7] R.P. Salvador, Accelerated cementitious matrices: hydration, microstructure and mechanical strength. Ph.D. Thesis (2016).
[8] I. Galobardes, S.H. Cavalaro, A. Aguado, T. Garcia, Estimation of the modulus of elasticity for sprayed concrete, Constr. Build. Mater. 53 (2014) 48–58, https://doi.org/10.1016/j.conbuildmat.2013.11.046.
[9] I. Galobardes, S.H. Cavalaro, C.I. Goodier, S. Austin, A. Rueda, Maturity method to predict the evolution of the properties of sprayed concrete, Constr. Build. Mater. 79 (2015) 357–369, https://doi.org/10.1016/j.conbuildmat.2014.12.038.
[10] R.P. Salvador, S.H.P. Cavalaro, R. Monte, A.D. de Figueiredo, Relation between chemical processes and mechanical properties of sprayed cementitious matrices containing accelerators, Cem. Concr. Comp. 79 (2017) 117–132, https://doi.org/10.1016/j.cemconcomp.2017.02.002.
[11] C. Herrera-Mesen, Evaluación de mezclas proyectadas: comportamiento y durabilidad. Ph.D. Thesis (2018).
[12] R.P. Salvador, S.H.P. Cavalaro, M. Cano, A.D. Figueiredo, Influence of spraying on the early hydration of accelerated cement pastes, Cem. Concr. Res. 88 (2016) 7–19, https://doi.org/10.1016/j.cemconres.2016.06.005.
[13] R. Siddique, M.I. Khan, Supplementary cementing materials, Springer (2011), https://doi.org/10.1007/978-3-642-17866-5.
[14] B. Lothenbach, K. Scrivener, R.D. Hooton, Supplementary cementitious materials, Cem. Concr. Res. 41 (2011) 1244–1256, https://doi.org/10.1016/j.cemconres.2010.12.001.
[15] A. Ishida, A. Araki, K. Yamamoto, M. Morioka, A. Hori, Application of blended cement in shotcrete to the environmental burden, Eng. Conf. Int. (2009).
[16] M.R.M. Saade, A. Passer, F. Mittermayr, A preliminary systematic investigation onto sprayed concrete's environmental performance, Proc. CIRP 69 (2018) 212–217, https://doi.org/10.1016/j.procir.2017.11.108.
[17] P. Sawoszczuk, M. Nokken, M. Jolin, Sustainable shotcrete using blast-furnace slag, Shotcrete (2013).
[18] R. Snellings, X-ray powder diffraction applied to cement, Pract. Guid. to Microstruct. Anal. Cem. Mater. (2015) 107–176, https://doi.org/10.1201/b19074-5.
[19] H.F.W. Taylor, Cement Chemistry, 2nd ed., Thomas Telford Publishing, 1997.
[20] P.C. Aïtcin, R.J. Flatt, Science and Technology of Concrete Admixtures, 1st ed., Woodhead Publishing, 2016.
[21] AENOR. UNE-EN 197-1:2011. Cement - Part 1: Composition, specifications and conformity criteria for common cements, 2011.
[22] ABNT. NBR NM 67:1998. Concrete - Slump test for the determination of the consistency, 1998.
[23] ABNT. NBR 9833:2008. Fresh concrete - Determination of the unit weight, yield and air content by the gravimetric test method, 2008.
[24] ABNT. NBR NM 47:2002. Concrete - Determination of air content of freshly mixed concrete - pressure method, 2002.
[25] J. Woodward, An introduction to geotechnical processes, 1st ed., Spon Press, 2005.
[26] AENOR. UNE-EN 14488-2:2007. Testing sprayed concrete - Part 2: Compressive strength of young sprayed concrete, 2007.
[27] EFNARC. European specification for sprayed concrete - Execution of spraying, 1999.
[28] R.P. Salvador, S.H.P. Cavalaro, I. Segura, A.D. Figueiredo, J. Pérez, Early age hydration of cement pastes with alkaline and alkali-free accelerators for sprayed concrete, Constr. Build. Mater. 111 (2016) 386–398, https://doi.org/10.1016/j.conbuildmat.2016.02.101.
[29] AENOR. UNE-EN 196-3. Methods of testing cement. Part 3: Determination of setting times and soundness, 2009.
[30] ASTM C 403/C 403M-08. Standard test method for time of setting of concrete mixtures by penetration resistance, 2008. doi:10.1520/E0336-11.the.
[31] AENOR. UNE-EN 12390-3. Testing hardened concrete. Part 3: Compressive strength of test specimens, 2009
[32] A.G. de la Torre, S. Bruque, J. Campo, M.A.G. Aranda, The superstructure of C_3S from synchrotron and neutron powder diffraction and its role in quantitative analysis, Cem. Conc. Res. 32 (2002) 1347–1356.
[33] T. Tsurumi, Y. Hirano, H. Kato, T. Kamiya, M. Daimon, Crystal structure and hydration of belite, Ceramic Trans. 40 (1994) 19–25.
[34] P. Mondal, J.W. Jeffery, The crystal structure of tricalcium aluminate, $Ca_3Al_2O_6$, Acta Cryst. B 31 (1975) 689–697.
[35] A.A. Colville, S. Geller, The crystal structure of brownmillerite, Ca_2FeAlO_5, Acta Cryst, B 27 (1971) 2311–2315.
[36] A.G. de la Torre, M.G. Lopez-Olmo, C. Alvarez-Rua, S.G. Granda, M.A.G. Aranda, Structure and microstructure of gypsum and its relevance to Rietveld quantitative phase analyses, Powder Diffr. 19 (2004) 240–246.
[37] R. Wartchow, Datensammlung nach der "learnt profile"-methode(LP) für calcit und vergleich mit der "background peak background"-methode (BPB), Zeit. Kristall. 186 (1989) 300–302.
[38] H.E. Petch, The hydrogen positions in portlandite, $Ca(OH)_2$, as indicated by the electron distribution, Acta Cryst. 14 (1961) 950–957.
[39] F. Goetz-Neunhoeffer, J. Neubauer, Refined ettringite structure for quantitative X-ray diffraction analysis, Powder Diffr. 21 (2006) 4–11.
[40] R. Allmann, Die,, Doppelschichtstruktur der plaettchenfoermigen Calcium-Aluminium-H Salze am Beispiel des $(CaO)3.Al_2O_3.CaSO_4(H_2O)_{12}$,, Neues Jahrbuch fuer Mineral. (1968) 140–144.
[41] T. Runcevski, R.E. Dinnebier, O.V. Magdysyuk, H. Poellmann, Crystal structures of calcium hemicarboaluminate and carbonated calcium hemicarboaluminate from synchrotron powder diffraction data, Acta Crystallogr., Sect. B: Struct. Sci. 68 (2012) 493–500.
[42] M. François, G. Renaudin, O. Evrard, A cementitious compound with composition $3CaO.Al_2O_3.CaCO_3.11H_2O$, Acta Crystallogr., Section C: Cryst. Struct. Commun. 54 (1998) 1214–1217.
[43] E.N. Maslen, V.A. Streltsov, N.R. Streltsova, N. Ishizawa, Y. Satow, Synchrotron X-ray study of the electron density in alpha-Al_2O_3, Acta Cryst. B 49 (1993) 973–980, https://doi.org/10.1107/S0108768193006901.
[44] M.H. Maciel, G.S. Soares, R.C.O. Romano, M.A. Cincotto, Monitoring of Portland cement chemical reaction and quantification of the hydrated products by XRD and TG in function of the stoppage hydration technique, Journ. Therm. Anal. Calor. doi: 10.1007/s10973-018-7734-5.
[45] R.P. Salvador, S.H.P. Cavalaro, A. Rueda, A.D. Figueiredo, Effect of cement composition on the reactivity of alkali-free accelerating admixtures for shotcrete. In: 7th International Symposium on Sprayed Concrete. Sandefjord, Norway, June/2014: pp. 350-360.
[46] R.P. Salvador, S.H.P. Cavalaro, M.A. Cincotto, A.D. de Figueiredo, Parameters controlling early age hydration of cement pastes containing accelerators for sprayed concrete, Cem. Concr. Res. 89 (2016) 230–248, https://doi.org/10.1016/j.cemconres.2016.09.002.
[47] K. Gong, C.E. White, Impact of chemical variability of ground granulated blast-furnace slag on the phase formation in alkali-activated pastes, Cem. Concr. Res. 89 (2016) 310–319, https://doi.org/10.1016/j.cemconres.2016.9.003.

[48] C. Maltese, C. Pistolesi, A. Bravo, T. Cerulli, D. Salvioni, M. Squinzi, Formation of nanocrystals of AFt phase during the reaction between alkali-free accelerators and hydrating cement: a key factor for sprayed concretes setting and hardening, RILEM Proc. F. Full J. TitleRILEM Proc. PRO 45 (2005) 329–338.

[49] R.P. Salvador, S.H.P. Cavalaro, I. Segura, G. Margarita, Relation between ultrasound measurements and phase evolution in accelerated cementitious matrices, Mater. Des. 113 (2017) 1–34, https://doi.org/10.1016/j.matdes.2016.10.022.

[50] C. Herrera-Mesen, R.P. Salvador, S.H.P. Cavalaro, A. Aguado, Effect of gypsum in sprayed cementtitious matrices: early age hydration and mechanical properties, Cem. Concr. Compos. 95 (2019) 81–91, https://doi.org/10.1016/j.cemconcomp.2018.10.015.

[51] N.J. Carino, H.S. Lew, The Maturity Method: From Theory to Application, in: P. C. Chang (Ed.), Struct. Congr. Expo., Washington DC, 2001: pp. 1–19. doi:10.1061/40558(2001)17.